

Seismic behavior of dumb-bell steel tube confined reinforced concrete piers

Xuhong Zhou, Haicui Wang*, Xuanding Wang, Jiepeng Liu

School of Civil Engineering, Chongqing University, Chongqing 400045, China

Key Laboratory of New Technology for Construction of Cities in Mountain Area (Chongqing University), Ministry of Education, Chongqing 400045, China

ARTICLE INFO

Keywords:

Dumb-bell RC pier
Dumb-bell steel tube confined RC pier
Seismic behavior
Lateral resistance model

ABSTRACT

To improve the strength and ductility of short reinforced concrete (RC) piers, dumb-bell steel tube confined reinforced concrete (DSTCRC) piers were proposed and studied, in which the dumb-bell steel tube is disconnected at the foundation and cap beam to avoid the difficulty of inserting steel tubes into RC members. In this paper, five DSTCRC piers and one reference dumb-bell RC pier were tested under pseudo-static loading. The test parameters included shear span-depth ratio (1.25 and 1.75), axial load ratio (0.12 and 0.24), and width of the web (75 mm and 100 mm). Because of the confinement and enhancement effect from the dumb-bell steel tube, failure modes of RC piers changed from shear failure to bending failure, and the strength, ductility, and energy dissipation capacity significantly improved. The seismic performance of DSTCRC piers improved slightly with the increasing axial load ratio and width of the web within the scope of this study. Shear failure of the concrete in the web cavity exhibited in DSTCRC specimens with a shear span-depth ratio of 1.25, but the lateral resistance increased by approximately 90% as the shear span-depth ratio decreased from 1.75 to 1.25 despite slight drops of the ductility ratio and ultimate displacement ratio. A simplified model considering the bending of RC cores and shear of steel webs and concrete web was proposed to predict the lateral resistance of DSTCRC piers, and the predicted results showed a good agreement with the test results.

1. Introduction

Large cross sections are commonly used for reinforced concrete (RC) piers to resist the lateral seismic load, resulting in heavy structural weight and wasting materials. In addition, RC piers have been demonstrated to be vulnerable to large earthquakes [1,2] as short RC piers, especially, without sufficient stirrups often suffer brittle failure. Concrete filled steel tube (CFST) piers, by contrast, have higher strength and better ductility benefitting from the composite effect between the steel tube and concrete [3–5]. The reduced cross-section and self-weight of piers, contribute to a saving in construction materials and labor. However, the application of CFST piers is often limited by the inherent difficulty of connections with the foundation or RC cap beam. The embedded depth of the steel tube at connections generally needs to be twice larger than of the cross-sectional diameter to meet the anchoring requirements, which is difficult for large-diameter CFST piers. In addition, the deeply-embedded steel tube will cause a complicated layout of reinforcement in the foundation [6–8].

To solve the aforementioned problems, an innovative composite bridge pier termed as Dumb-bell Steel Tube Confined Reinforced Concrete (DSTCRC) pier is proposed in this study. As shown in Fig. 1, a DSTCRC pier consists of a dumb-bell steel tube and infilled reinforced

concrete, where the dumb-bell steel tube is made up of two circular steel tubes and two steel web plates. It should be noted that gaps are left between the dumb-bell steel tube and the adjacent foundation/cap beam to simplify the construction process of connections and alleviate the flexural demand on the joint [9]. In a DSTCRC pier, the flexural strength is provided by the inner concrete and reinforcing bars. Of using dumb-bell steel tube include: (1) the compressive strength and ultimate compressive strain of concrete core are improved due to lateral confinement of the steel tubes, thus enhanced the deformability of flexural plastic hinge; (2) the shear strength of squat piers is enhanced owing to the steel web plates shearing; (3) dumb-bell steel tube can be used as a formwork for casting concrete in construction. The dumb-bell steel tube terminates at the connections and carries no direct axial load, therefore, the probability of local buckling is significantly reduced. As a result, high-strength and thin-walled steel tubes could be used in DSTCRC piers to optimize the economic benefits.

The steel tube confined reinforced concrete (STCRC), also known as steel-jacketed reinforced concrete (SJRC) or tubed reinforced concrete (TRC), originated from a retrofit method for non-ductile RC piers in which a steel jacket is added to the potential plastic hinge region. Priestley and Park et al. [10] studied the seismic behavior of RC bridge piles with continuous and discontinuous steel tubes and revealed that

* Corresponding author at: School of Civil Engineering, Chongqing University, Chongqing 400045, China.

E-mail address: wanghaicui@cqu.edu.cn (H. Wang).

Nomenclature

Notions

A_c	cross-sectional area of the specimen
A_{sp}	area of the steel web plate
A_{cw}	area of the concrete web
D	diameter of the circular steel tube
d_c	width of the web
f_{cc}	confined concrete strength
f_{co}	unconfined concrete strength
$f_{y,sp}$	yield strength of the steel web plate
f_y	yield strength of longitudinal reinforcement
f_u	ultimate strength of steel plate
h	height of dumb-bell section
h_1	distance between centers of two circular tubes in the dumb-bell section
h_2	height of the steel web plate
L	length of the specimen
L_e	distance between the lateral loading point and the top surface of the foundation
M_b	bending capacity of the RC core corresponding the applied axial load
M_1	bending capacity of circular STCRC corresponding to N_1
P_y	yield load
P_u	peak load
$P_{0.85}$	ultimate load

$P_{u,pre}$	lateral load by predicted the proposed model
P_b	lateral resistance from bending of RC core
P_{ss}	lateral resistance from shear of steel web plate
P_{sc}	lateral resistance from shear of concrete web
t_c	wall-thickness of the circular steel tube
t_s	wall-thickness of the steel web plate
N	axial load
N_1	axial load carried by the circular STCRC on the compression side at critical condition of bearing capacity
N_2	yield tensile forces of LW
N_3	yield tensile forces of LC
n	axial load ratio
R	$P_{u,pre}$ to P_u ratio
x_{cu}	distance between the extreme compression fiber and the neutral axis
λ	shear span-depth ratio
μ	displacement ductility coefficient
ε_{cu}	ultimate concrete compressive strain
σ_h	transverse stress of steel tube
σ_v	longitudinal stress of steel tube
σ_r	shear stress of steel tube
σ_m	von Mises stress of steel tube
Δ_{yc}	test yield displacement
Δ_y	yield displacement
Δ_u	peak displacement
$\Delta_{0.85}$	ultimate displacement
φ	ultimate drift ratio

the piles with discontinuous steel tubes exhibited excellent seismic performance, and their strength and stiffness had almost no reduction under cyclic loading. Priestley et al. [11,12] conducted comparative seismic tests on four circular RC piers and four retrofit piers with steel tubes not extending into the cap beam and foundation. The results showed that all the RC piers suffered brittle shear failure and low ductility, while the steel-jacketed piers exhibited good seismic performance with displacement ductility factors greater than 8. Aboutaha et al. [13] combined drilling bolts with rectangular steel jackets to enhance the confinement effect of non-ductile RC columns. Xiao et al. [14] developed a retrofit method using welded rectilinear steel jackets and stiffeners, which significantly improved the strength and ductility of square and rectangular RC columns. Lubiewski et al. [15] proposed a method to increase the ductility of column-bent cap connections of Alaska bridges by disconnecting the semi-embedded steel tubes from the bent cap with a 51 mm wide gap and enlarging the bent caps in the joint region. Montejó et al. [9] investigated the seismic performance of circular RC-filled steel tube piles/columns multi-span bridge bents,

where the steel tubes extended into the foundation at the bottom end but terminated at the top connection with the cap beam. The design of the bridge bents was generally governed by the top hinge of the column and strain-based limit states were proposed based on the experimental results. Billah et al. [16] evaluated the seismic performance of multi-column bents retrofitted by different materials, i.e. steel tube, carbon fiber reinforced polymer (CFRP), engineered cementitious composite (ECC), and RC jacketing. The results showed that the bridge piers retrofitted by steel tube had minimal residual deformation. Stephens et al. [17] proposed some CFST piers-prefabricated RC cap beam connections for rapid bridge construction, in which the connection with steel tube terminated at the cap beam is similar to STCRC. Such a connection outstands due to its reliable performance and construction convenience.

In building structures, the STCRC columns have also received extensive attention. Tomii et al. [18] firstly investigated the shear strength and ductility of TRC columns, and TRC columns tended to have more excellent seismic behavior compared with RC columns. Sakino and Sun et al. [19,20] studied the square STCRC short columns under axial compression and showed that the corner longitudinal reinforcements did not affect the failure mode of concrete and a stress-strain curve of concrete confined by square steel tube as presented. Sun et al. [21,22] studied the square STCRC short columns with different shear span ratios and proposed a method to calculate the lateral bearing capacity of square STCRC short columns failed in shear and bending failure. Aboutaha et al. [23] carried out a comparative test on the hysteretic behavior of rectangle STCRC and RC members. The results show that the seismic performance of rectangular STCRC columns was better than RC with difference concrete strengths and axial load ratios. Han et al. [24] studied six circular STCRC columns and six square STCRC columns under constant load combined with cyclic lateral load, showing that the energy dissipation ability of circular STCRC columns was much higher than that of square STCRC. Zhou and Liu et al. [25] studied the seismic behavior and shear strength of circular STCRC short columns with a shear span ratio of 1.5. In the test, the circular STCRC short columns suffered bending failure or bending-shear failure. Zhou et al. [26] investigated the connections between RC beams and square

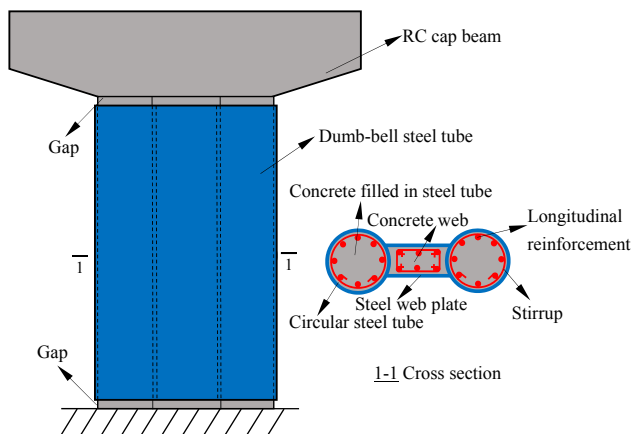


Fig. 1. Dumb-bell steel tube confined reinforced concrete piers.

Table 1
Details of specimens.

Specimens	L (mm)	h (mm)	D (mm)	d (mm)	t_c (mm)	t_s (mm)	h_1 (mm)	h_2 (mm)	LC	LW	TC	TW	n	λ	N (kN)
DRC	800	571	200	100	—	—	371	—	4 Φ 10	4 Φ 10	Φ 8@100	Φ 8@200	0.12	1.75	259
DSTCRC1	800	571	200	100	2	2	371	196	4 Φ 10	4 Φ 10	Φ 8@100	Φ 8@200	0.12	1.75	259
DSTCRC2	800	571	200	75	2	2	371	185	4 Φ 10	2 Φ 10	Φ 8@100	Φ 8@200	0.12	1.75	244
DSTCRC3	800	571	200	75	2	2	371	185	4 Φ 10	2 Φ 10	Φ 8@100	Φ 8@200	0.24	1.75	489
DSTCRC4	800	800	200	75	2	2	600	415	4 Φ 10	3 Φ 10	Φ 8@100	Φ 8@200	0.12	1.25	300
DSTCRC5	800	800	200	75	2	2	600	415	4 Φ 10	3 Φ 10	Φ 8@100	Φ 8@200	0.24	1.25	600

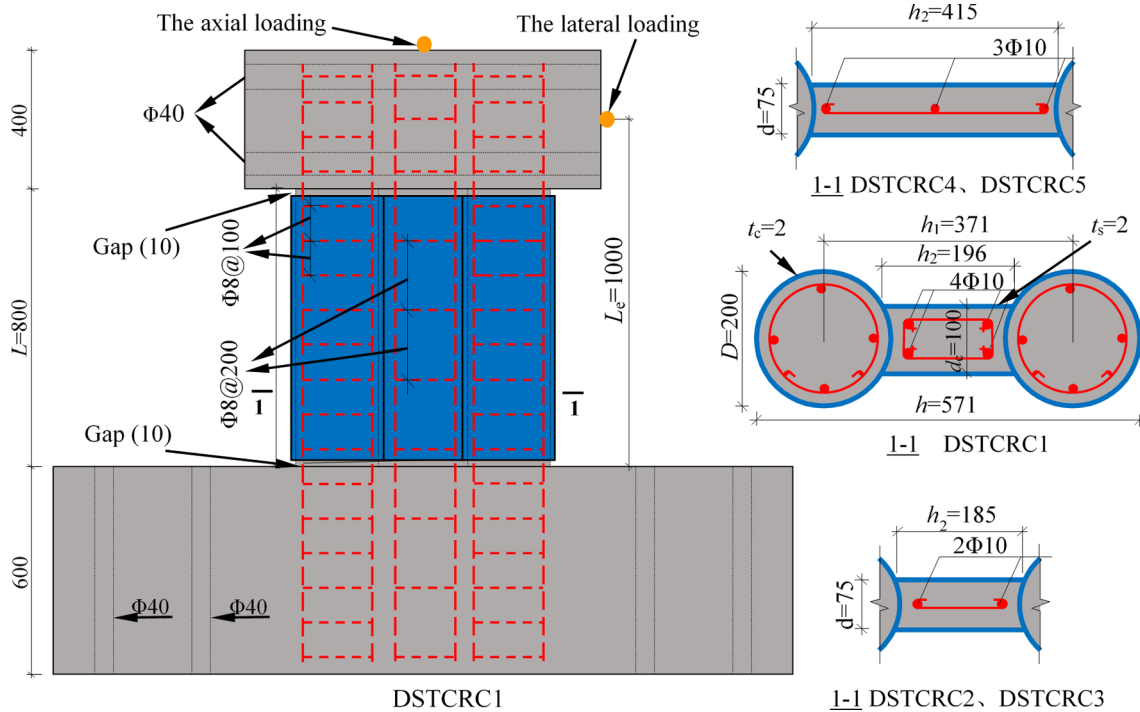


Fig. 2. Details of the DSTCRC specimens (unit:mm).

Table 2
Material properties of the steel components.

Steel type	Steel plate thickness (mm)		Diameter (mm)		Yield strength (MPa)
	Nominal	Measured	Nominal	Measured	
Steel plate	2.00	1.88	—	—	315
Longitudinal reinforcement	—	—	10.0	9.80	473
Stirrups	—	—	8.00	7.65	457

STCRC columns under axial compression. The test results showed that all specimens had high load-carrying capacity and ductility. When properly designed, connections between RC beams and square TRC columns can achieve higher axial resistance and better ductility performance than the CFST column.

Previous studies mainly focused on the behavior of STCRC with circular, square, and rectangular sections. The circular STCRC is well confined but its moment of inertia and shear strength are relatively small. The square or rectangular STCRC makes better use of the shear strength of the steel tube, but the tube confinement is insufficient. The DSTCRC pier is proposed in consideration of the following advantages: (1) the dumb-bell cross-section has a large moment of inertia, and the RC cores at the two flanges are effectively confined by the circular steel tubes, resulting in high bearing capacity against axial compression and

bending moment, as well as good rotation ability; (2) the steel web plates significantly improve the shear strength and energy consumption ability of short piers by forming a diagonal tensile stress field. Therefore, the DSTCRC has a promising application prospect in short piers or ultra-short piers that are subjected to large seismic forces during earthquakes.

In this paper, a pseudo-static test is conducted on five DSTCRC short piers and one reference dumb-bell RC (DRC) short pier, and the investigated parameters include shear span-depth ratio, axial load ratio, and width of the web. The failure modes, load-displacement hysteresis curves, mechanical properties, and stress development of the dumb-bell steel tubes are described and discussed herein. Based on the test results, a simplified lateral resistance model of DSTCRC piers was proposed.

2. Test program

2.1. Specimens

In total, six specimens were prepared and tested under combined constant axial load and cyclic lateral load, including five DSTCRC specimens and one DRC reference specimen. The investigated parameters are the shear span-depth ratio, axial load ratio, and width of the web. The details of each specimen are shown in Table 1, where L is the length of the pier, h is the height of dumb-bell section, D is the diameter of the circular steel tube, d is the width of the web (distance between the inner surface of the two steel web plates), t_c is the wall-thickness of the circular steel tube, t_s is the wall-thickness of the steel web plate, h_1 is the distance between centers of two circular tubes, h_2 is the height of the steel web plate, LC and LW are the longitudinal reinforcement in the circular steel tubes and web, respectively, where, for example, 4Φ10 represents 4 reinforcing bars with a nominal diameter of 10 mm, TC and TW are the transverse reinforcement in the concrete of circular steel tubes and web, respectively, where, for example, Φ 8@100 means that 8 mm diameter transverse steel bars were evenly spaced along the length at 100 mm, n is the axial load ratio determined by Eq. (1), and λ is the shear span-depth ratio determined by Eq. (2).

$$n = N / (f_{co} A_c) \quad (1)$$

$$\lambda = \frac{L_e}{h} \quad (2)$$

where N is the axial load, f_{co} is the axial compressive strength of the concrete, A_c is the cross-sectional area of the specimen, and L_e is the distance between the lateral loading point and the top surface of the foundation (Fig. 2).

Fig. 2 shows the plan views and reinforcement and steel details of the specimens. Each specimen has a bottom RC foundation block of 1800 mm (length) × 800 mm (width) × 600 mm (height) with eight 40 mm diameter vertical holes for fixing, and a top RC large beam of 1000 mm (length) × 400 mm (width) × 400 mm (height) with four 40 mm diameter transverse holes for connecting loading devices. The circular steel tubes and the steel web plates in the dumb-bell cross-sections are fabricated from the same batch of steel plates with a nominal wall-thickness of 2 mm, and they are connected by the fillet welds. The dumb-bell steel tube is disconnected at 10 mm from both the pier ends to avoid carrying direct axial loads. The longitudinal bars are embedded into the foundation and the top large beam with sufficient anchor length. Besides, the reference Specimen DRC is identical to Specimen DSTCRC1 except for the absence of a dumb-bell steel tube.

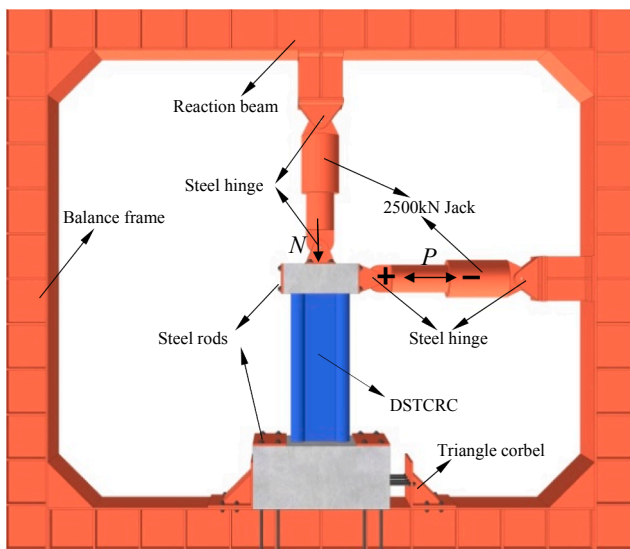


Fig. 3. Test set-up.

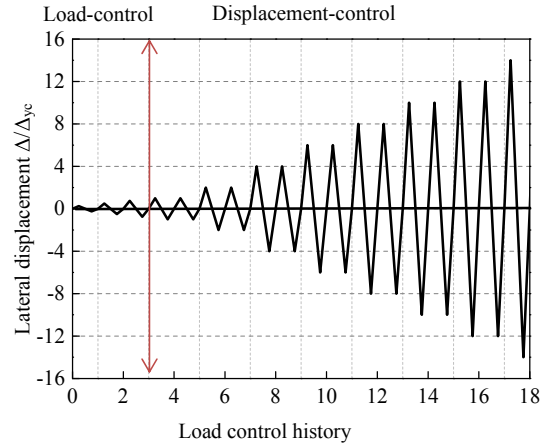


Fig. 4. Cyclic loading history.

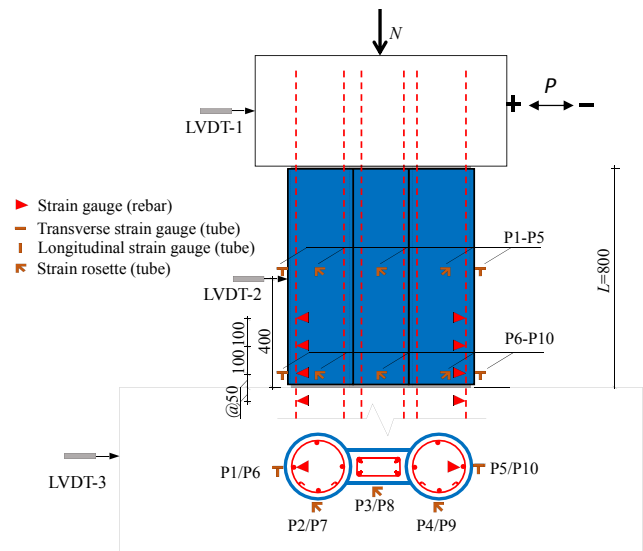


Fig. 5. Layout of LVDTs and strain gauges.

Specimen DSTCRC1 except for the absence of a dumb-bell steel tube.

2.2. Material properties

Tensile coupons were tested according to the Chinese Standard GB50010/T228-2010 [27,28] to determine the mechanical properties of the steel plates and reinforcements used in the specimens, as shown in Table 2. All specimens were cast using the same batch of ready-mixed concrete and the layered concrete pouring process was adopted to ensure a more uniform and densified concrete finish. Concrete cubes (150 mm × 150 mm × 150 mm) and prisms (150 mm × 150 mm × 300 mm) were prepared and cured under the same condition to determine the average cubic concrete strength ($f_{cu,150} = 35.2$ MPa) and elastic modulus ($E_c = 39472$ MPa) [29]. Based on the cubic strength, the average axial compressive strength of concrete used in the calculation ($f_{co} = 29.03$ MPa) is obtained according to the Model Code 1990 (CEB-FIP 1991) [30].

2.3. Test set-up

The self-balancing frame was used for the quasi-static seismic loading, as shown in Fig. 3. The bottom foundation of the specimen was fixed to the frame by eight 38 mm diameter steel rods and triangle corbels. A 2500 kN jack for applying the axial loads (N) and a 2500 kN jack for applying the lateral loads (P) were installed to the reaction

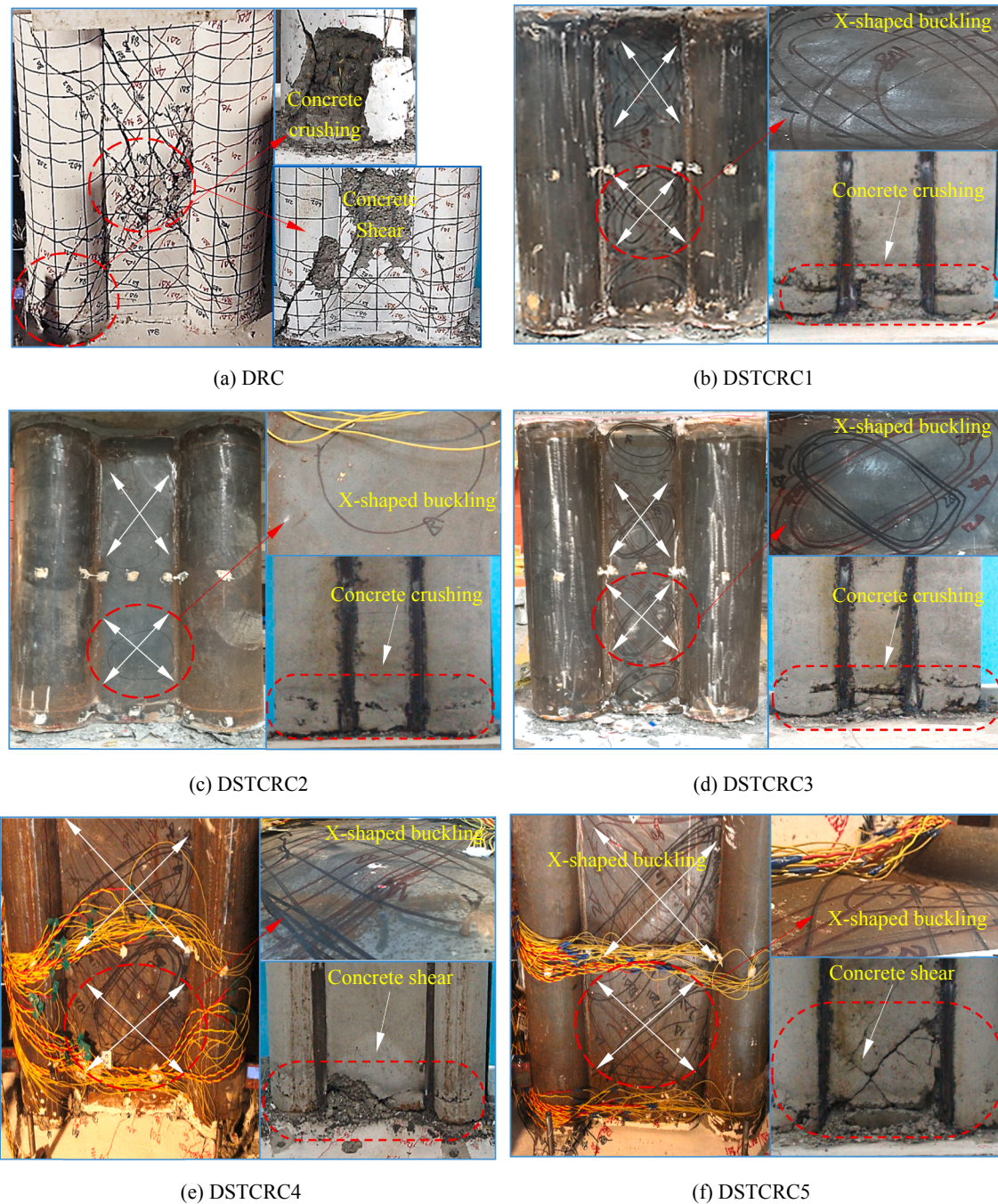


Fig. 6. Failure modes of the specimens.

beams and the top beam of the specimen was connected to the top beam using four 38 mm diameter steel rods by steel hinges.

The cyclic lateral loads (P) were applied after reaching the target axial loads (N). The cyclic lateral loading history consisted of an elastic stage and an inelastic stage (JGJ/T 101-2015) [31]. The elastic stage was conducted under load-control till yielding load, with an interval of 1/3 yielding load [31]. The test yield displacement (Δ_{yc}) is estimated by the first distinguishable stiffness degradation of the hysteretic curve observed during the test. The yielding load is corresponding to Δ_{yc} . After the yielding load, the displacement-control method was adopted

in the inelastic stage (Fig. 4), and each displacement level was cycled twice until the specimen failed or the bearing capacity of the specimens reduced to less than 85% of the peak bearing capacity [31]. The load was applied at a rate of 5 kN/s and 1 mm/s in the elastic and inelastic stages, respectively.

2.4. Measuring system

Load cells were mounted next to the jacks to measure the applied loads. Three linear variable differential transformers (LVDT) were

Table 3
Damage characteristics at different loading stages of the specimens (unit:mm).

DRC	Observations		Failure Mode	
$\Delta = 2.3$	Initial diagonal cracks		Shear failure	
$\Delta = 3.6$	X-shaped diagonal cracks in concrete web & initial horizontal cracks at cylinder end			
$\Delta = 14.4$	Peak load & outermost rebar yielded & slight spalling of the concrete cover			
$\Delta = 21.6$	85% of the peak load & X-shaped cracks developed to the circle & spalling of the concrete web cover & crush of concrete at the cylinder end			
DSTCRC1	DSTCRC2	DSTCRC3	Observations	Failure Mode
$\Delta = 2.0$	$\Delta = 2.3$	$\Delta = 2.5$	Initial horizontal cracks at the gap	RC bending failure and steel webs shear failure
$\Delta = 4.0$	$\Delta = 4.6$	$\Delta = 5.0$	X-shaped diagonal buckling in steel web plates & outermost rebar yielded	
$\Delta = 14.9$	$\Delta = 18.4$	$\Delta = 22.4$	Peak load & X-shaped buckling developed to the circular steel tube	
Steel tube removed			85% of the peak load & concrete crushing and spalling at the pier bottom	
DSTCRC4	DSTCRC5	Observations		Failure Mode
$\Delta = 2.0$	$\Delta = 2.4$	Initial horizontal cracks at the gap		RC bending failure, steel webs shear failure and concrete web shear failure
$\Delta = 4.0$	$\Delta = 4.8$	X-shaped diagonal buckling in steel web plates & outermost rebar yielded		
$\Delta = 22.9$	$\Delta = 28.6$	Peak load & X-shaped buckling developed to the circular steel tube & spalling of the web concrete		
Steel tube removed		85% of the peak load & concrete crushing and spalling at the pier bottom & diagonal cracks at the bottom of the concrete web		

employed to measure the lateral displacement of the specimens, in which LVDT-1 was at the top of the specimen where the lateral load was applied, LVDT-2 was at the middle of the pier, and LVDT-3 was at the specimen foundation (Fig. 5). The measured results of LVDT-3 indicated that the displacement of the specimen foundation relative to the self-balancing frame was generally less than 1 mm during the whole loading process. The strains at 10 measuring points of the dumb-bell steel tubes including 5 ones (P1-P5) at the mid-length section and 5 ones (P6-P10) at the bottom section were recorded using strain gauges or strain rosettes (Fig. 5). Eight strain gauges are arranged to the left and right outmost rebar at 100 mm intervals to monitor the strain development of reinforcement within the plastic hinge region (Fig. 5).

3. Results and discussion

3.1. Test observations and failure modes

Fig. 6 and Table 3 show the failure modes of all the specimens and list their main damage characteristics at different loading stages, where Δ is the displacement measured by LVDT-1 (Fig. 5). Serious shear failure with a great number of diagonal cracks and spalling of concrete was observed in the reference RC specimen. Compared with the failure mode of Specimen DRC, the RC cores in DSTCRC piers were effectively confined and enhanced by the dumb-bell steel tubes, thus the failure mode was changed from shear failure to bending failure. Specimens DSTCRC1- DSTCRC 3 had a similar failure mode, i.e., yielding of longitudinal reinforcement, crushing of concrete within the plastic hinge region, and yielding of steel web plates in the diagonal tension direction, being characterized by bending failure of RC core and shear failure of steel web plates. Because of the increase of the height of the web, the shear failure of the infilled concrete in the cavity was occurred in Specimens DSTCRC4 and DSTCRC5, and Specimen DSTCRC5 suffered more serious damage due to the higher axial load ratio. Therefore, the failure mode of Specimens DSTCRC4 and DSTCRC5 could be characterized by bending failure of RC cores and shear failure of steel web plates and concrete web. It should be noted that the foundation was robust enough despite a few cracks that were found on the top surface of the foundation.

3.2. Load versus displacement hysteresis curves

Fig. 7 shows the lateral load (P) - lateral displacement (Δ) hysteresis curves of specimens. Pinch effect is observed in all the P - Δ hysteresis curves, which is caused by the opening and closure of concrete cracks and the relative slip between the steel tube and concrete. Compared with the Specimen DRC, the DSTCRC specimens have better deformability and dissipate more earthquake energy as their full P - Δ hysteresis loops covering bigger areas. In addition, the yield points of the utmost longitudinal reinforcements of the specimens are marked in Fig. 7. For Specimen DRC, the reinforcement yielded at the peak load. For all the DSTCRC specimens, the yield of the reinforcement and the initial buckling of steel web plates approximately happened simultaneously, indicating that the bond between steel web plates and inner concrete was overcome when the longitudinal reinforcements yielded, and the diagonal tensile stress field of the steel web plates was gradually developed to resist the lateral loads and improve the energy dissipation performance of the specimens.

3.3. Envelop curves and comparative analysis

Fig. 8 shows envelop curves obtained from the P - Δ hysteretic curves. The following observations can be found: (1) the initial elastic stiffness of the Specimen DSTCRC1 is similar to that of Specimen DRC, while the elastoplastic stiffness, peak load, ultimate deformability and ductility of Specimen DSTCRC1 are higher than those of Specimen DRC (Fig. 8(a)); (2) the load-carrying capacity and ductility of the DSTCRC piers increase with the increasing n within the studied parameters (Fig. 8(b)); (3) the lateral resistance of the DSTCRC piers increases significantly with the decreasing shear span-depth ratio, but the ductility slightly decreases (Fig. 8(b)).

Table 4 lists some mechanical properties calculated from the envelope curves in Fig. 8 (average of two loading directions), where P_y is the yield load, Δ_y is the yield displacement [32], P_u is the peak load, Δ_u is displacement corresponding to P_u , $P_{0.85}$ is the ultimate load, $\Delta_{0.85}$ is displacement corresponding to $P_{0.85}$, μ is the displacement ductility coefficient ($\mu = \Delta_u/\Delta_y$), and φ is the ultimate drift ratio ($\varphi = \Delta_{0.85}/L_e$). The yield displacement of the specimens is determined by the geometric graphic method [32], the ultimate state is defined as the moment when

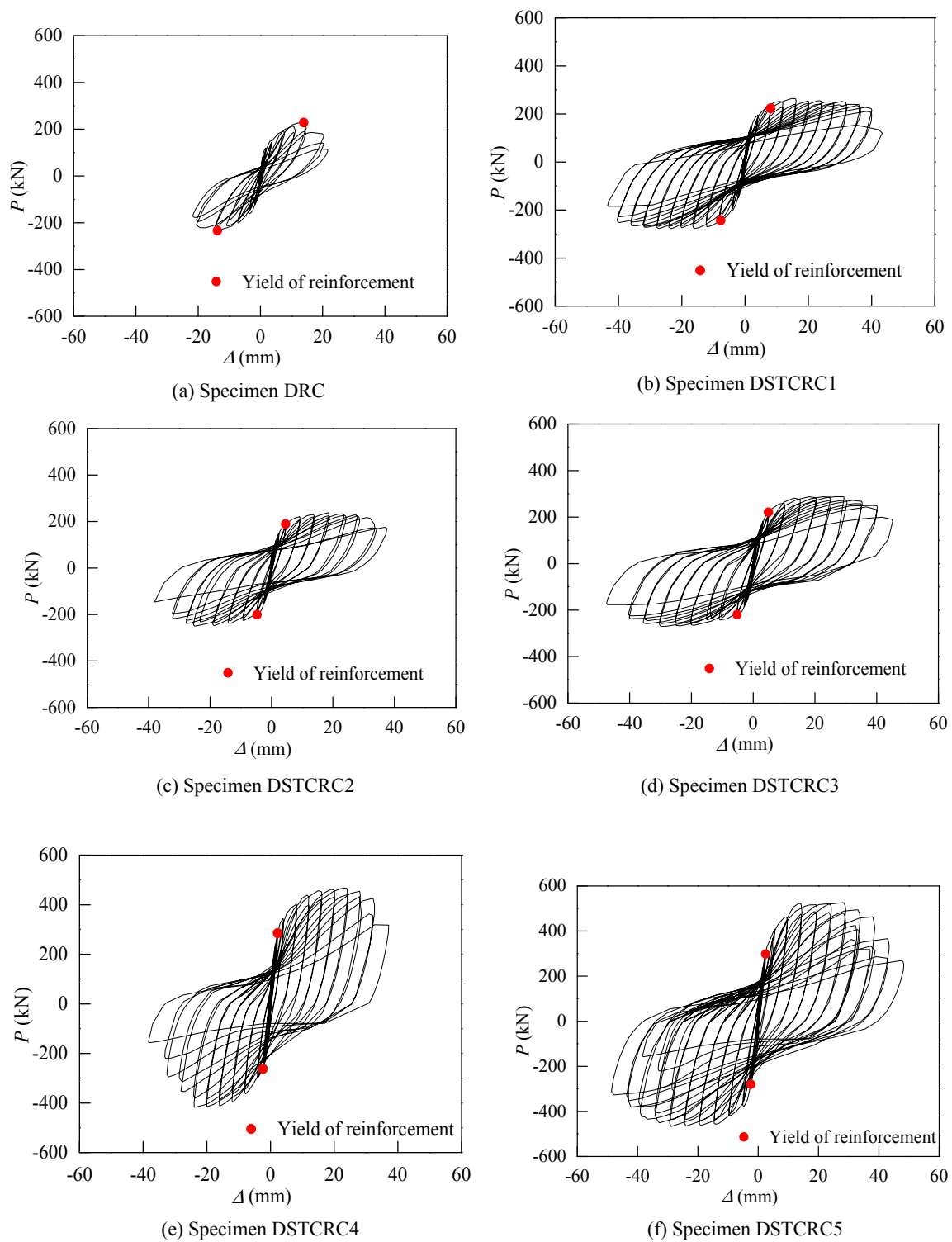


Fig. 7. Lateral load versus lateral displacement hysteresis curves.

the lateral load reduces to 85% of P_u . The lateral load-carrying capacity of Specimen DSTCRC1 (RC bending failure) was approximately 16% higher than that of Specimen DRC (RC shear failure), and the displacement ductility coefficient and ultimate drift ratio of Specimen

DSTCRC1 are approximately double of those of Specimen DRC. Increasing the width of the web from 75 mm (Specimen DSTCRC2) to 100 mm (Specimen DSTCRC1) slightly improved the P_u of DSTCRC specimens by about 10%. To further explain the influence of axial load

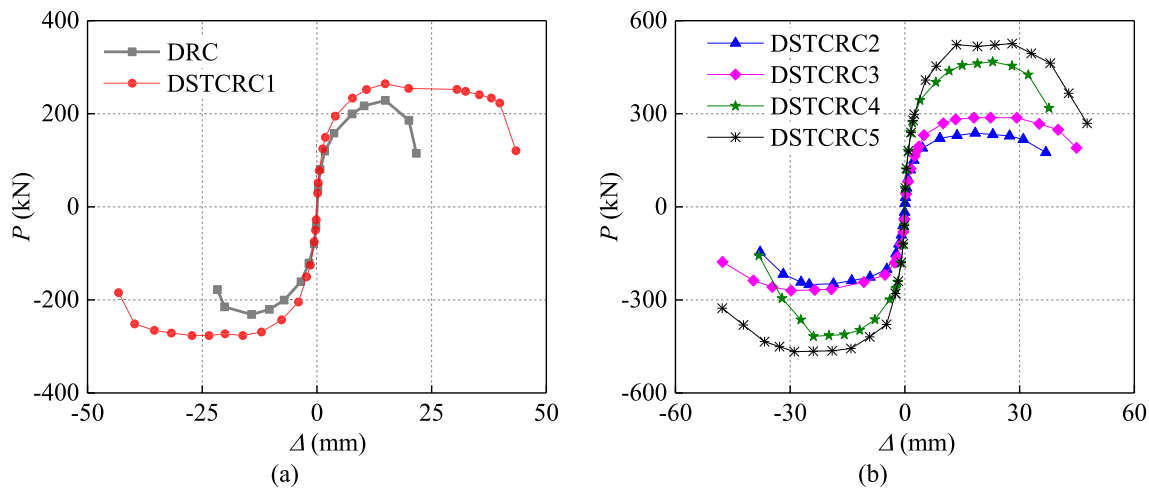


Fig. 8. Comparison of load versus displacement envelop curves.

Table 4

Characteristic values of all specimens.

Specimens	n	λ	P_y (kN)	Δ_y (mm)	P_u (kN)	Δ_u (mm)	$P_{0.85}$ (kN)	$\Delta_{0.85}$ (mm)	μ	φ
DRC	0.12	1.75	184.30	6.27	228.69	14.93	194.39	19.45	3.10	1.95%
DSTCRC1	0.12	1.75	213.44	5.92	264.35	14.88	224.70	38.89	6.57	3.89%
DSTCRC2	0.12	1.75	198.34	5.90	237.67	18.40	202.02	33.96	5.76	3.40%
DSTCRC3	0.24	1.75	242.38	6.54	287.40	22.39	244.29	40.26	6.16	4.03%
DSTCRC4	0.12	1.25	381.00	6.61	467.50	22.95	397.38	33.86	5.12	3.39%
DSTCRC5	0.24	1.25	430.81	6.92	526.37	28.06	447.42	39.00	5.64	3.90%

ratio and shear span-depth ratio on the seismic performance of DSTCRC specimens in a more direct-viewing way, bar graphs are provided in Fig. 9, which indicates that the axial load ratio within the scope of this study played a positive role in improving seismic performance, and the lateral resistance was approximately increased by 90% with a slight decrease of ductility ratio and ultimate drift ratio as the shear span-depth ratio decreasing from 1.75 to 1.25.

3.4. Load versus stress curves of circular steel tube and steel web plate

Based on the recorded strains of the dumb-bell steel tube, the stress development is studied using the elastic-plastic analysis method proposed in Ref. [33]. Fig. 10 shows the analysis results of a typical specimen, where σ_v , σ_h , σ_t , and σ_m represent the longitudinal stress, transverse stress, shear stress, and von Mises stress, respectively, and P1-3 and P6-8 represent the measure points (Fig. 5).

The axial force was gradually transferred from concrete to steel tube at P1. The concrete expanded after bearing the axial compression, arousing the confinement of the circular steel tube. Along with the axial compression of circular concrete transferred from P6 to P1 gradually, the concrete expansion became larger and the stress of P1 circular steel tube increased faster. The longitudinal stress of circular steel tube was greater than the transverse stress, and the deformation of circular steel tube and concrete at mid-height section was almost the same so that the longitudinal stress was higher than that at the bottom. The transverse stress of the circular steel tube at P2(P7) was similar to that at P1(P6). The longitudinal stress at P2 was smaller than that at P1, and the longitudinal stress at P7 was similar to that at P6. The shear stress at P2 and P7 increased gradually from the initial loading stage to the peak load when the circular steel tube yielded.

As for P3(P8), the bond between the steel web plate and concrete began to be overcome locally after the cyclic lateral loading. The steel web plate buckled when the steel web plate separated from the concrete web and reached the yield displacement of the specimen. Since that, the bulge area of the steel plate under the cyclic lateral load gradually increased, which alternated repeatedly with two 45° diagonal waveform. Eventually, the X-shaped bulges appeared and the steel web plate yielded near the peak load.

4. Lateral resistance model of DSTCRC piers

According to the analysis of specimens failure mechanism, the lateral resistance ($P_{u,pre}$) of a DSTCRC pier is contributed by the following three components (Fig. 11): (1) P_b from the bending of RC core; (2) P_{ss} from the shear of steel web plate (tension in diagonal direction); (3) P_{sc} from the shear of concrete web, being determined by,

$$P_{u,pre} = \begin{cases} P_b + 2P_{ss} & \text{concrete web failed in bending (DSTCRC1 - 3)} \\ P_b + 2P_{ss} + P_{sc} & \text{concrete web failed in shear (DSTCRC4,5)} \end{cases} \quad (3)$$

(1) Bending of RC core

A fiber model is established to analyze the flexural behavior of the RC core (Fig. 12), in which the concrete in the circular steel tubes adopts a constitutive model of steel tube confined concrete [34], the concrete in the web cavity adopts a constitutive model of plain concrete [28], and the steel reinforcements are assumed to be elastic perfectly-plastic. Besides, the strain of the extreme compression concrete fiber is the ultimate concrete compressive strain ϵ_{cu} , which is determined by

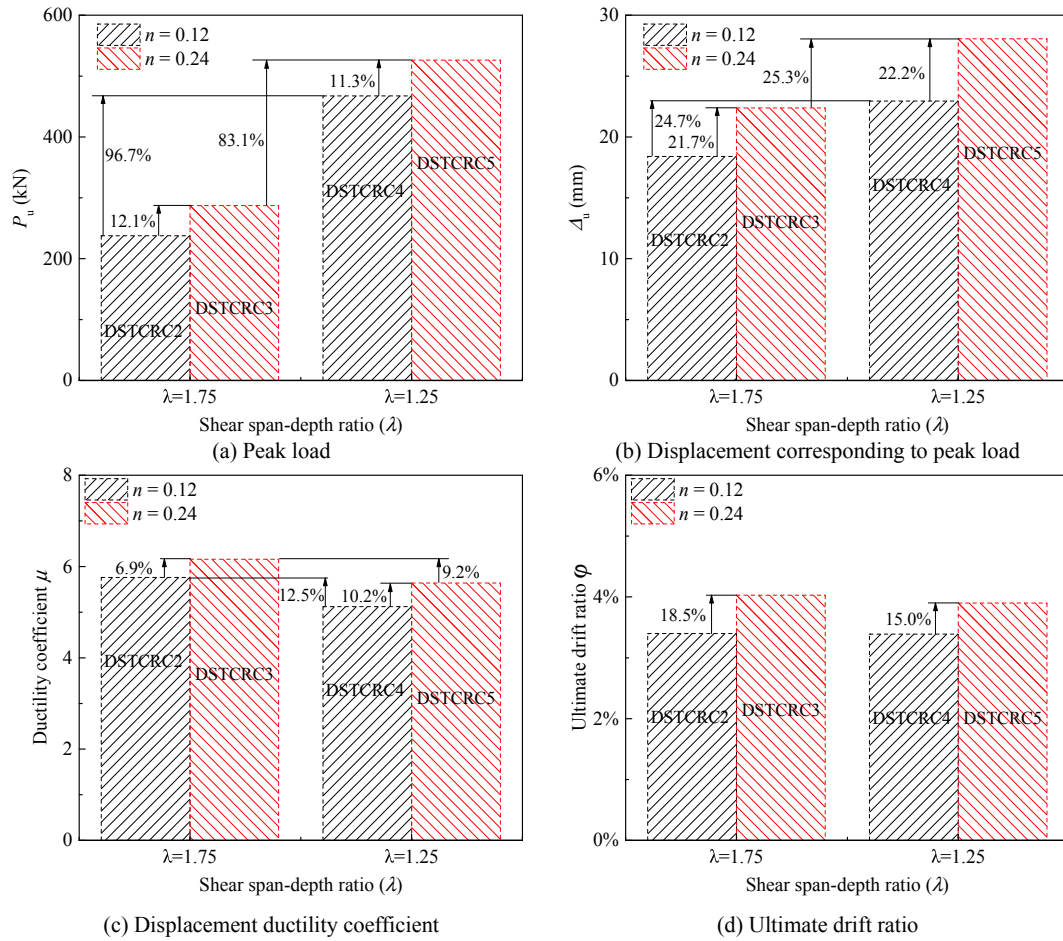


Fig. 9. Influence of shear span-depth ratio and axial load ratio on key performance indexes.

Eq. (4) proposed in reference [34], where f_{cc} is confined concrete strength.

$$\varepsilon_{cu} = \begin{cases} 0.018 \times (f_{cc}/f_{co} - 1) + 0.003 & f_{co} \leq 50 \text{ MPa} \\ 0.029 \times (f_{cc}/f_{co} - 1) + 0.003 & f_{co} > 50 \text{ MPa} \end{cases} \quad (4)$$

Based on the axial force (N)-moment (M) interaction relationship of the RC cores in the tested DSTCRC specimens obtained by the fiber model (Fig. 13), the flexural strength (M_b) of the RC core corresponding to the applied axial load was determined. Using M_b and assuming that the bending failure of the RC core was located at the section $D/2$ away from the top surface of the foundation, the lateral resistance P_b contributed by the bending of RC core can be estimated by,

$$P_b = \frac{M_b - N\Delta_u}{(L_e - D/2)} \quad (5)$$

However, the aforementioned calculating method of M_b is too complicated. Based on the analysis of fiber model, the bending of the RC core can be simplified as follows, 1) the circular STCRC component on the compression side is in the bending limit state with the axial load of N_1 and the bending moment of M_1 ; 2) all the reinforcements in the concrete web (LW, Table 1) and the tensile circular STCRC (LC, Table 1) yielded with the tensile forces of N_2 and N_3 , respectively. Based on the bending equilibrium of the simplified model, P_b is calculated by,

$$P_b = \frac{(N + N_2)h_1/2 + N_3h_1 + M_1}{L_e - D/2} \quad (6)$$

where N_2 and N_3 can be calculated by multiplying the yield strength of the reinforcements by the corresponding areas, and M_1 is the bending capacity of a circular STCRC column carrying the axial force of N_1 ($N_1 = N + N_2 + N_3$), which can be determined according to the literature [34]. As shown in Fig. 14, P_b predicted by Eq. (7) agrees well with that predicted by Eq. (6), which demonstrates the availability of the simplified bending model.

(2) Shear of the steel web plates

The shear capacity of the steel web plates in DSTCRC piers can be estimated by half of the shear strength of steel plates with four fixed sides because only the two sides of the steel web plates are fixed [35]. In this study, the model of four-sided fixed shear wall proposed by Berman et al. [35] was modified to predict the shear strength of the steel webs in DSTCRC, thus P_{ss} can be calculated by,

$$P_{ss} = 0.25f_{ysp}A_{sp} \quad (7)$$

where, f_{ysp} is yield strength of the steel web plate, A_{sp} is the area of the steel web plate.

(3) Shear of the concrete web

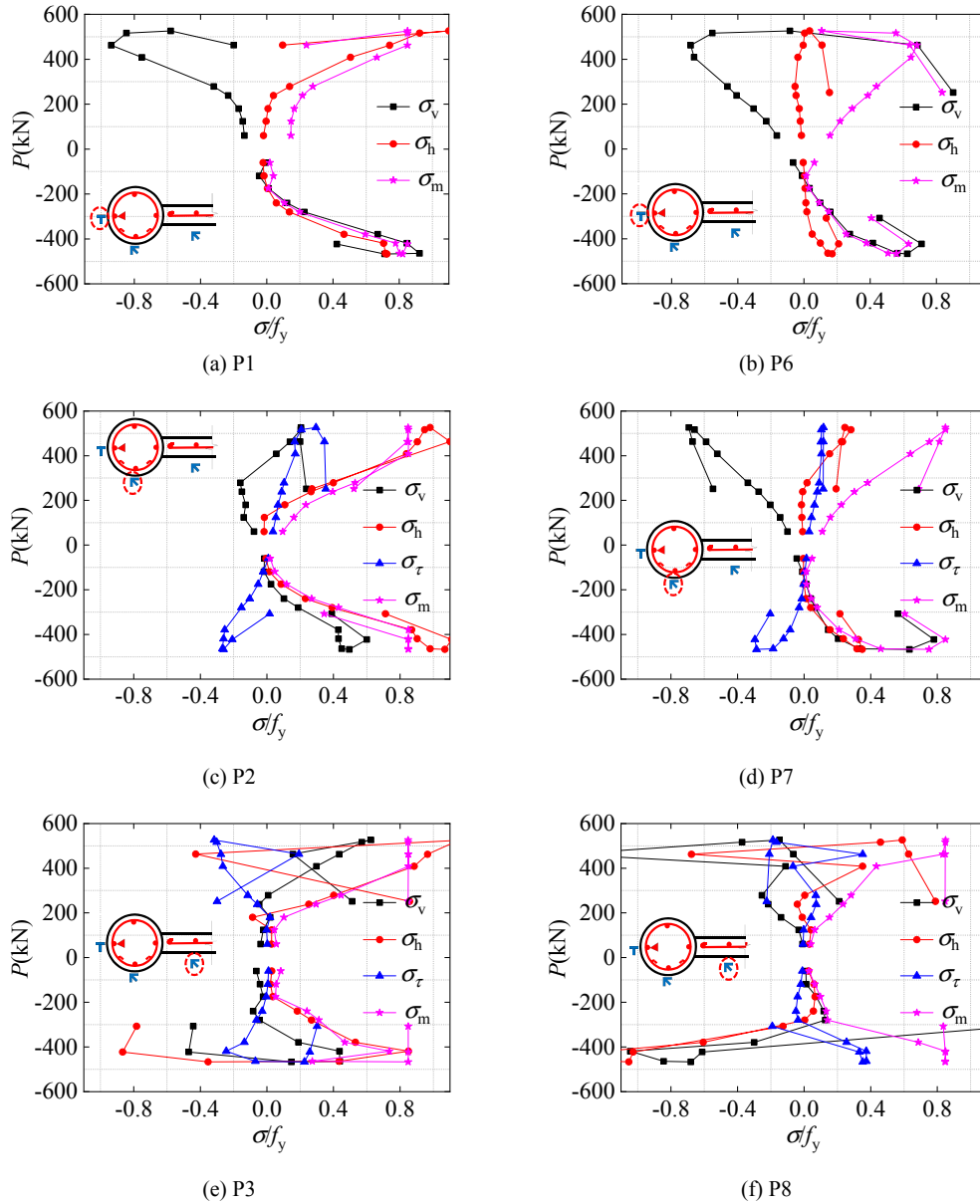


Fig. 10. Lateral load versus stress curves of circular steel tube and steel web plate of Specimen DSTCRC5.

Since the axial compressive loads of bridge piers are relatively small and mainly carried by the circular STCRC on the compression side, the influence of axial loads on the shear capacity of concrete web can be ignored. According to ACI318-14[36], the lateral resistance P_{sc} provided by the shear resistance of concrete web is determined by,

$$P_{sc} = 0.17\sqrt{f_{co}}A_{cw} \quad (8)$$

where, A_{cw} is the area of the concrete web.

Table 5 and Fig. 15 show the predictions of the lateral resistance model and the test results, in which R is the $P_{u,pre}$ to P_u ratio in Eq. (9). The difference between the predicted results and the test results is within 5%. The bending of the RC core contributes the most to the lateral resistance of DSTCRC piers. P_h of Specimens DSTCRC1-3 is about $0.7P_u$, and that of the Specimens DSTCRC4,5 is about $0.6P_u$. The shear

of concrete webs has a limited effect on P_u , accounting for less than 6%.

$$R = \frac{P_{u,pre}}{P_u} \quad (9)$$

5. Conclusions

In this paper, 5 DSTCRC piers and 1 reference dumb-bell RC pier were tested under pseudo-static load. The test parameters included shear span-depth ratio (1.25 and 1.75), axial load ratio (0.12 and 0.24), and width of the web (75 mm and 100 mm). The failure modes, load-displacement hysteresis curves, mechanical properties, and stress development of the dumb-bell steel tubes are described and discussed in detail. Based on the test results, a simplified lateral resistance model of

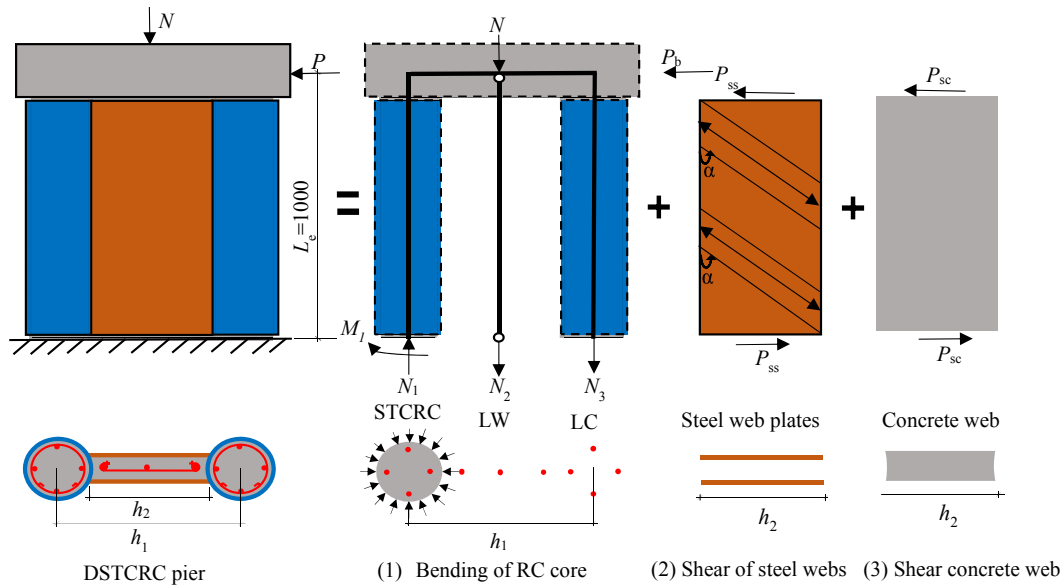


Fig. 11. Lateral resistance model of DSTCRC piers.

DSTCRC piers was proposed. The main conclusions are as follows:

- (1) Because of the confinement and enhancement effect from the dumb-bell steel tube, the failure modes of RC piers were changed from shear to bending. Compared with the reference DRC specimen, the DSTCRC specimen with the same parameters has better deformability and dissipate more earthquake energy, as the peak load increasing by about 16%, and the displacement ductility coefficient and ultimate drift ratio increasing by nearly one time.
- (2) The bending failure of the RC core and the shear failure of steel web plates were observed in all DSTCRC specimens. For specimens with a shear span-depth ratio of 1.25, the concrete web was also failed in shear. Another important test observation is that the yield of longitudinal reinforcements happened just at the moment of the initial buckling of steel web plates, implying a redistribution of the internal forces.
- (3) Increasing the axial load ratio and width of the web within the

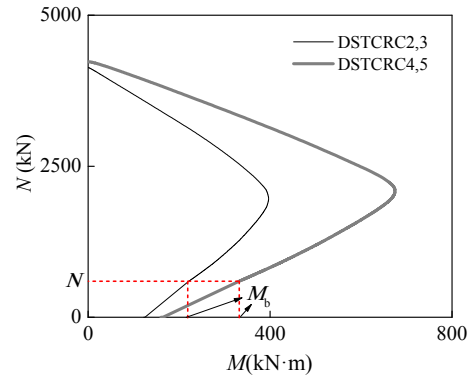


Fig. 13. Predicted N - M interaction curves of RC cores by fiber model.

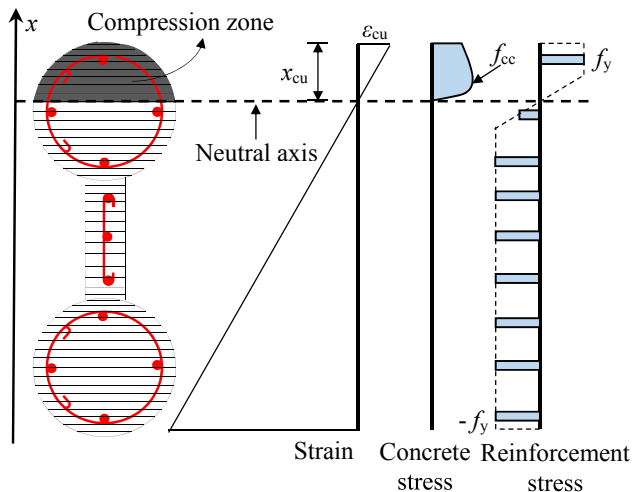


Fig. 12. Fiber model of the RC core.

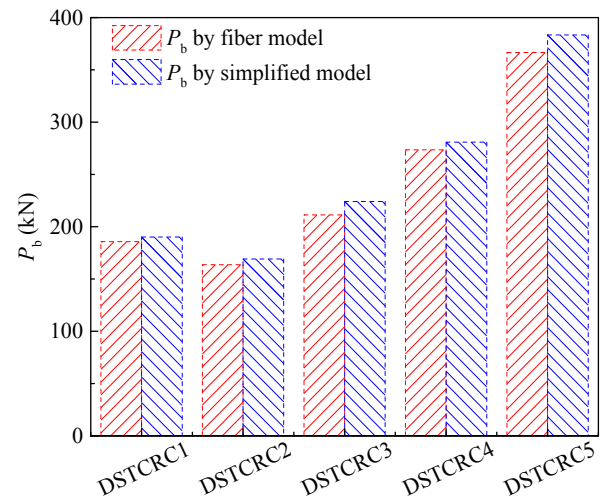


Fig. 14. Comparison of P_b predicted by the fiber model and the simplified model.

Table 5
Comparisons of experimental results P_u and predicted P_b , P_{ss} , and P_{sc} by simplified model.

Specimens	P_b by Eq. (6) (kN)	$2P_{ss}$ by Eq. (7) (kN)	P_{sc} by Eq. (8) (kN)	$P_{u,pre}$ by Eq. (3) (kN)	P_u (kN)	R
DRC	—	—	—	—	228.7	—
DSTCRC1	190.1	61.7	16.5	251.8	264.4	0.953
DSTCRC2	169.2	58.3	12.3	227.5	237.7	0.957
DSTCRC3	224.2	58.3	12.3	282.5	287.4	0.983
DSTCRC4	280.9	130.7	28.2	439.8	457.5	0.961
DSTCRC5	383.4	130.7	28.2	542.3	526.4	1.030

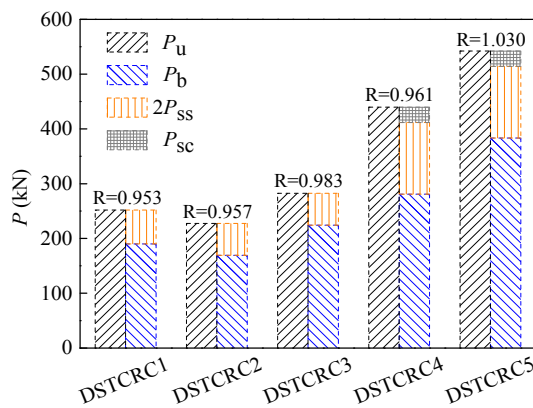


Fig. 15. Comparison of experimental results P_u and predicted P_b , P_{ss} , and P_{sc} by simplified model.

scope of this study slightly improved seismic performance of DSTCRC piers, while the lateral resistance was approximately increased by 90% with a slight decrease of ductility ratio and ultimate drift ratio as the shear span-depth ratio decreasing from 1.75 to 1.25.

- (4) The seismic resistance of a DSTCRC pier is contributed by the bending of RC core, the diagonal tension of steel web plates, and the shear of concrete web, in which the bending of the RC core accounts for about 60%~70%, and the shear of concrete webs only accounts for less than 6%. A simplified lateral resistance model of DSTCRC piers was proposed, and the predicted results agree well with the test results.

CRediT authorship contribution statement

Xuhong Zhou: Conceptualization, Formal analysis, Funding acquisition, Project administration, Supervision, Validation, Writing - original draft, Writing - review & editing. **Haicui Wang:** Conceptualization, Data curation, Investigation, Methodology, Project administration, Software, Validation, Writing - original draft, Writing - review & editing. **Xuanding Wang:** Methodology, Supervision, Validation, Writing - original draft, Writing - review & editing. **Jiepeng Liu:** Conceptualization, Investigation, Project administration, Supervision, Validation, Writing - original draft, Writing - review & editing.

Declaration of Competing Interest

The authors declared that they have no conflicts of interest to this work. We declare that we do not have any commercial or associative interest that represents a conflict of interest in connection with the work submitted.

Acknowledgement

This research is made possible through the financial support from the National Natural Science Foundation of China (#51438001, #51622802), to which the authors are very grateful.

References

- [1] Priestley MJN, Seible F, Calvi GM. Seismic design and retrofit of bridges. New York: John Wiley & Sons; 1996.
- [2] Chang KC, Chang DW, Tsai MH, Sung YC. Seismic performance of highway bridges. Earthq Eng Seismol 2000;2(1):55–77.
- [3] Kitada T. Ultimate strength and ductility of state-of-the-art concrete-filled steel bridge piers in Japan. Eng Struct 1998;20(4–6):347–54.
- [4] Marson J, Bruneau M. Cyclic testing of concrete-filled circular steel bridge piers having encased fixed-based detail. J Bridge Eng 2004;9(1):14–23.
- [5] Bruneau M, Marson J. Seismic design of concrete-filled circular steel bridge piers. J Bridge Eng 2004;9(1):24–34.
- [6] Hsu HL, Lin HW. Improving seismic performance of concrete-filled tube to base connections. J Constr Steel Res 2006;62(12):1333–40.
- [7] Stephens MT, Lehman DE, Roeder CW. Design of CFST column-to-foundation/cap beam connections for moderate and high seismic regions. Eng Struct 2016;122:323–37.
- [8] Xu W, Han LH, Li W. Seismic performance of concrete-encased column base for hexagonal concrete-filled steel tube: experimental study. J Constr Steel Res 2016;121:352–69.
- [9] Montejó LA, González-Román LA, Kowalsky MJ. Seismic performance evaluation of reinforced concrete-filled steel tube pile/column bridge bents. J Earthq Eng 2012;16(3):401–24.
- [10] Priestley MJN, Park RJT. Concrete filled steel tubular piles under seismic loading. Proceedings of the International Specialty Conference on Concrete Filled Steel Tubular Structures. 1985. p. 96–103.
- [11] Priestley MJN, Seible F, Xiao Y, et al. Steel jacket retrofitting of reinforced concrete bridge columns for enhanced strength-part 1: Theoretical considerations and test design. ACI Struct J 1994;91(4):394–405.
- [12] Priestley MJN, Seible F, Xiao Y. Steel jacket retrofitting of reinforced concrete bridge columns for enhanced shear strength-Part 2: Test results and comparison with theory. ACI Struct J 1994;91(5):537–51.
- [13] Aboutaha RS, Engelhardt MD, Jirsa JO, et al. Retrofit of concrete columns with inadequate lap splices by the use of rectangular steel jackets. Earthq Spectra 1996;12(4):693–714.
- [14] Xiao Y, Wu H. Retrofit of reinforced concrete columns using partially stiffened steel jackets. J Struct Eng 2003;129(6):725–32.
- [15] Lubiewski MC, Silva PF, Chen G. Retrofit of column-bent cap connections of Alaska bridges for seismic loadings: damage evaluation. Struct Congr 2006: Struct Eng Publ Saf 2006:1–13.
- [16] Billah AHM, Alam MS. Seismic performance evaluation of multi-column bridge bents retrofitted with different alternatives using incremental dynamic analysis. Eng Struct 2014;62:105–17.
- [17] Stephens MT, Berg LM, Lehman DE, et al. Seismic CFST column-to-precast cap beam connections for accelerated bridge construction. J Struct Eng 2016;142(9):04016049.
- [18] Tomii M, Sakino K, Watanabe K. Lateral load capacity of reinforced concrete short columns confined by steel tube. Proceedings of the International Specialty Conference on Concrete-Filled Steel Tubular Structures. 1985. p. 19–26.
- [19] Sakino K, Sun YP, Toshihiko N. Behaviour of Concrete Confined in Square Steel Tube under Axial Compression, Part 1: Details of Test Specimens [in Japanese]. Summaries of Technical Papers of Annual Meeting Architectural Institute of Japan, Structures II 1991:215–6.
- [20] Sun YP, Sakino K, Toshihiko N. Behaviour of Concrete Confined in Square Steel Tube under Axial Compression, Part 2: Stress-Strain Curve of Confined Concrete [in Japanese]. Summaries of Technical Papers of Annual Meeting Architectural Institute of Japan, Structures II 1991:217–8.
- [21] Sun YP, Sakino K. Earthquake-resisting performance of R/C columns confined by square steel tube, Part 3: effects of shear span ratio of column. J Struct Construct Eng ALJ 2001;547:129–36.
- [22] Sun YP, Sakino K, Aklan MA. Method for calculating ultimate moment of concrete columns retrofitted by square steel tube [in Japanese]. Proceedings of The Japan Concrete Institute 1996, 18-2:131–6.
- [23] Aboutaha RS, Machado R. Seismic resistance of steel confined reinforced concrete (SCRC) columns. Struct Design Tall Build 1998;7(3):251–60.
- [24] Han LH, Yao GH, Chen ZB, et al. Experimental behaviours of steel tube confined concrete (STCC) columns. Steel Compos Struct 2005;5(6):459–84.
- [25] Zhou X, Liu J. Seismic behavior and shear strength of tubed RC short columns. J Constr Steel Res 2010;66(3):385–97.
- [26] Zhou XH, Li BY, Gan D, et al. Connections between RC beam and square tubed-RC column under axial compression: Experiments. Steel Compos Struct 2017;23(4):453–64.
- [27] GB/T 228.1-2010 Metallic materials-Tensile testing-Part1:Method of test at room temperature. Standards Press of China, Beijing; 2010. [in Chinese].
- [28] GB 50010. (2010). Code for design of concrete structures. Chinese Architecture Industry Press, Beijing; 2010. [in Chinese].
- [29] GB 50081. (2002) Standard for test method of mechanical properties on ordinary

- concrete. China architecture & building press, Beijing; 2003. [in Chinese].
- [30] CEB-FIP. Comité Euro-International du Béton–Fédération International de la Précontrainte. Thomas Telford, London;1991.
- [31] JGJ/T. 2015. Specification for seismic test of buildings. Chinese Architecture Industry Press, Beijing; 2015. [in Chinese].
- [32] Park R. Ductility evaluation from laboratory and analytical testing. Proceedings of the 9th world conference on earthquake engineering, Tokyo-Kyoto, Japan. 1988; 8: 605–16.
- [33] Cheng GZ, Zhou XH, Liu JP, Frank Chen Y. Seismic behavior of circular tubed steel-reinforced concrete column to steel beam connections. *Thin Walled Struct* 2019;138:485–95.
- [34] Wang X, Liu J, Zhang S. Behavior of short circular tubed-reinforced-concrete columns subjected to eccentric compression. *Eng Struct* 2015;105:77–86.
- [35] Berman J, Bruneau M. Plastic analysis and design of steel plate shear walls. *J Struct Eng* 2003;129(11):1448–56.
- [36] ACI318-14 Building code requirements for structural concrete and commentary. Farmington Hills, MI: American Concrete Institute; 2014.